

The Ω Dependence in the Equations of Motion

Adi Nusser & Jörg M. Colberg

Max Planck Institut für Astrophysik, Karl Schwarzschild Str. 2, D-85748 Garching b. München, Germany

24 June 2018

ABSTRACT

We show that the equations of motion governing the evolution of a collisionless gravitating system of particles in an expanding universe can be cast in a form which is *almost* independent of the cosmological density parameter, Ω , and the cosmological constant, Λ . The new equations are expressed in terms of a time variable $\tau \equiv \ln D$, where D is the linear rate of growth of density fluctuations. The weak dependence on the density parameter is proportional to $\epsilon = \Omega^{-0.2} - 1$ times the difference between the peculiar velocity (with respect to τ) of particles and the gravity field (minus the gradient of the potential), or, before shell-crossing, times the sum of the density contrast and the velocity divergence. In a 1-dimensional collapse or expansion, the equations are fully independent of Ω and Λ before shell-crossing. In the general case, the effect of this weak Ω dependence is to enhance the rate of evolution of density perturbations in dense regions. In a flat universe with $\Lambda \neq 0$, this enhancement is less pronounced than in an open universe with $\Lambda = 0$ and the same Ω . Using the spherical collapse model, we find that the increase of the *rms* density fluctuations in a low Ω universe relative to that in a flat universe with the same linear normalization is $\sim 0.01\epsilon(\Omega) \langle \delta^3 \rangle$, where δ is the density field in the flat universe. The equations predict that the smooth average velocity field scales like $\Omega^{0.6}$ while the local velocity dispersion (*rms* value) scales, approximately, like $\Omega^{0.5}$. High resolution N-body simulations confirm these results and show that density fields, when smoothed on scales slightly larger than clusters, are insensitive to the cosmological model. Halos in an open model simulation are more concentrated than halos of the same M/Ω in a flat model simulation.

Key words: cosmology: theory – dark matter – large scale structure of Universe

1 INTRODUCTION

The cosmological background determines the growth rate of matter density fluctuations. This is the result of two effects. First, the initial conditions are specified in terms of the density contrast field $\delta \equiv \rho(\mathbf{x})/\rho_b - 1$. Therefore the actual density, $\rho(\mathbf{x})$, which dictates the dynamical evolution, as can be seen for example from the spherical top-hat model, depends on the mean matter density, ρ_b . The second effect comes about simply because the mean matter density varies with time according to the assumed cosmological model. This in turn translates into a dependence of the evolution of the fluctuation field δ on the parameters of the cosmological model: the density parameter, Ω , and the cosmological constant, Λ . Here we focus on the following aspect of the dependence of dynamics on the cosmological background. Starting from an initial density fluctuation field and a given amplitude of the evolved field, we address the question: how do the evolved peculiar velocity and density fields depend on the parameters Ω and Λ ? In the linear (e.g. Peebles 1980) and in the Zel'dovich quasilinear (Zel'dovich 1970) approxima-

tions, once an initial density fluctuation field is evolved to a given amplitude, it does not contain any information on the parameters Ω and Λ . In these approximations, the peculiar velocity field is simply proportional to $f(\Omega, \Lambda)$ where f is the so-called linear growth factor. This result is easy to understand. In the linear approximation, the density fluctuations are merely amplified by a time dependent factor, D . In the Zel'dovich approximation, the displacement vector is the product of the initial gravity field and the function D . Moreover, second order perturbation theory calculations (e.g. Bouchet *et al.* 1992) have shown that moments of the density fluctuation field are very insensitive to Ω and Λ . Finally, in the highly nonlinear regime, N-body simulations (e.g. Davis *et al.* 1985) show that the final matter distribution in simulations with the same initial conditions changes very little as the parameters of the cosmological background are varied. Significant differences between flat and open models are found only in the cores of what are identified as rich clusters in these simulations. These results have proved useful in analyzing observations of the large scale structure. Nusser and Dekel (1993), for example, used N-body simulations to argue that a recovery of the initial

arXiv:astro-ph/9705121v1 16 May 1997

density fluctuations from the observed galaxy distribution is almost independent of $f(\Omega, \Lambda)$, where as a recovery from the observed peculiar velocity field is sensitive to the assumed Ω . They applied their reconstruction method to the POTENT compilation of the peculiar velocity data and to the 1.2 Jy IRAS survey and concluded that $\Omega > 0.3$ with high confidence. Bernardeau *et al.* (1995) used second order perturbation theory to argue that the reduced skewness of the divergence of the peculiar velocity field is inversely proportional to f , in accordance with the scaling implied by the Zel'dovich approximation. They found that the measured skewness is consistent with Ω of about unity.

Here we aim at a better understanding of the dependence of the equations of motion on the cosmological parameters. In section 2 we write the equations of motion in a form which is almost independent of the background cosmology. We discuss the Ω dependence in toy-models in section 3. In section 4, we use high resolution N-body simulations to investigate in detail the differences in the matter distribution in flat and open models. We conclude with a summary and discussion in section 5.

2 ALMOST Ω INDEPENDENT EQUATIONS OF MOTION

We restrict our treatment to the case of a matter dominated universe with a cosmological constant, i.e, we assume that the total mean density is $\rho_{tot} = \rho_b + \Lambda/3$ where $\rho_b(t)$ is the matter contribution and Λ is the cosmological constant. We use the standard notation in which, $a(t)$ is the scale factor, $H(t) = \dot{a}/a$ is the time dependent Hubble factor, $\Omega = \rho_b(t)/\rho_c(t)$ and $\lambda = \Lambda/3H^2$ where $\rho_c = 3H^2/8\pi G$ is the critical density. Let \mathbf{x} and $\mathbf{v} = d\mathbf{x}/dt$ be the position and peculiar velocity of a particle in comoving coordinates. The equations of motion are: the continuity equation

$$\frac{d\delta}{dt} + (1 + \delta) \nabla \cdot \mathbf{v} = 0, \quad (1)$$

the Euler equation of motion,

$$\frac{d\mathbf{v}}{dt} + 2H\mathbf{v} = -\frac{3}{2}\Omega\nabla\phi, \quad (2)$$

and the Poisson equation,

$$\Delta\phi = \delta. \quad (3)$$

Note that we have defined $\phi \equiv 2\Phi_g/3\Omega$ where Φ_g is the peculiar gravity potential in comoving coordinates. Equations (1), (2) and (3) together with the Friedman equations for the background quantities Ω and a fully specify the dynamics of pressure free density fluctuations. The scale factor, a , can be solved for using the Friedman equation

$$\left(\frac{da}{dt}\right)^2 = \frac{8\pi}{3}G\rho_b a^2 + \frac{\Lambda}{3}a^2 - k, \quad (4)$$

where $k = +1, -1$ and 0 correspond, respectively, to closed, open or flat universes. Energy conservation, $\rho_b a^3 = const$,

yields $\Omega = c_0/H^2 a^3$ where $c_0 = \Omega_0 H_0^2 a_0^3$ and the subscript 0 denotes quantities at the present time. Therefore, energy conservation and (4) yield

$$\Omega = \frac{c_0}{c_0 + \frac{\Lambda}{3}a^3 + ka}. \quad (5)$$

The hubble factor, H , can be eliminated from these equations by working with a new time variable $p \equiv \ln a$. We define a new ‘‘velocity’’ $\boldsymbol{\alpha} \equiv d\mathbf{x}/dp = H^{-1}\mathbf{v}$. In these new variables, the Poisson equation remains unaltered while the continuity and Euler equations become

$$\frac{d\delta}{dp} + (1 + \delta) \nabla \cdot \boldsymbol{\alpha} = 0, \quad (6)$$

$$\frac{d\boldsymbol{\alpha}}{dp} + (1 - q) \boldsymbol{\alpha} = -\frac{3}{2}\Omega\nabla\phi, \quad (7)$$

where $q(p) = \Omega/2 - \lambda$ is the time dependent deceleration parameter and we have used $dH/dp = -(1 + q)H$ to derive (7).

Attempting to eliminate Ω from (7) we further make an additional transformation from the time variable p to τ defined by

$$\tau = \ln D(p), \quad (8)$$

where D is the linear growing density mode determined by the equation,

$$\frac{d^2 D}{dt^2} + 2H \frac{dD}{dt} - \frac{3}{2}\Omega H^2 D = 0. \quad (9)$$

Analytic solutions to (9) can be found in Heath (1977). Expressing (7) in terms of τ defining the ‘‘velocity’’ $\boldsymbol{\beta} \equiv d\mathbf{x}/d\tau$, continuity equation is

$$\frac{d\delta}{d\tau} - (1 + \delta)\theta = 0, \quad (10)$$

and the Euler equation is

$$f^2 \frac{d\boldsymbol{\beta}}{d\tau} + \left[\frac{df}{d\tau} + (1 - q)f \right] \boldsymbol{\beta} = -\frac{3}{2}\Omega\nabla\phi, \quad (11)$$

where, $\theta = -\nabla \cdot \boldsymbol{\beta}$, and $f = d\tau/dp$ is the linear growth factor which relates density contrast, δ , to the divergence of the peculiar velocity field, \mathbf{v} , in the linear regime. For $\lambda = 0$, a good approximation* for f is $f \approx \Omega^{0.6}$ (Peebles 1980). For $\lambda \neq 0$, Lahav *et al.* (1991) found that $f \approx \Omega^{0.6} + \lambda(1 + \Omega/2)/70$. Therefore, for reasonable values of the cosmological constant we neglect the dependence of f on λ in the approximate forms for f (Lahav *et al.* 1991). Note that the velocity $\boldsymbol{\beta} = \mathbf{v}/(Hf)$. In the Zel'dovich approximation, this is the

* For $\lambda = 0$, the function f satisfies $(1 - \Omega) \frac{df}{d\ln\Omega} - (1 - \frac{\Omega}{2})f + \frac{3}{2}\Omega - f^2 = 0$, which to first order in $1 - \Omega$ yields $f \approx \Omega^{4/7}$ for $\Omega \approx 1$ (see also Lightman & Schechter 1990). However, the general solution to this equation is better fitted by $f \approx \Omega^{0.6}$ for $\Omega < 0.7$. A fit which works well for $0.05 < \Omega < 1$ is $f = \Omega^{\frac{4}{7} + \frac{(1-\Omega)^3}{20}}$.

displacement vector of a particle from its initial to present position. Using (9), we find

$$\frac{df}{dp} + (1 - q)f = \frac{3}{2}\Omega - f^2, \quad (12)$$

so the Euler equation (11) is

$$\frac{d\boldsymbol{\beta}}{d\tau} - \boldsymbol{\beta} - \frac{3}{2}[1 + \epsilon(\Omega)](\mathbf{g} - \boldsymbol{\beta}) = 0, \quad (13)$$

where

$$\epsilon(\Omega) \equiv \frac{\Omega}{f^2} - 1 \approx \Omega^{-0.2} - 1, \quad (14)$$

and we have defined $\mathbf{g} = -\nabla\phi$. The weak dependence on Ω in (13) through $\epsilon(\Omega)$ couples to the difference between the velocity, $\boldsymbol{\beta}$, and the gravity field, \mathbf{g} . Since $\Omega \sim 1$ at early times, initially the function ϵ almost vanishes, thus, any changes in the dynamics as a result of this weak dependence on Ω occur at later times.

In virialised regions, the acceleration of a particle is dominated by the gravity field \mathbf{g} . It is easy to see that by neglecting the terms involving the velocity in (13) and working with a new time variable with respect to which the velocity is $(1 + \epsilon)^{-1/2}\boldsymbol{\beta} \approx \Omega^{0.1}\boldsymbol{\beta}$ we obtain an Euler equation which is independent of Ω . This velocity is approximately equal to the comoving peculiar velocity divided by $H\Omega^{0.5}$. This scaling with Ω is not surprising since the virial theorem implies that the *rms* value of the physical velocities in virialised regions with a given density contrast has similar scaling with Ω . Note however that the scaling is only approximate since the density profile of virialised objects has some dependence on Ω .

3 Ω DEPENDENCE IN TOY MODELS

It is clear from the form of (13) that the source term which drives the evolution is larger for lower Ω . Therefore we expect to see more evolved clustering in a low Ω universe than in an $\Omega = 1$ universe with the same initial conditions and linear normalisation. It is instructive to investigate the effect of the term ϵ in cases of special symmetry. Consider first the spherical expansion or collapse before the occurrence of shell crossing. This case illustrates the effect of changing Ω in the before shell-crossing. In cases of special symmetry, we find it easier to solve directly for δ and θ rather than for \mathbf{g} and $\boldsymbol{\beta}$. Therefore we take the divergence of (13) and use the Poisson equation to obtain

$$\frac{d\theta}{d\tau} - \theta - \Pi^2 - \frac{3}{2}[1 + \epsilon(\Omega)](\delta - \theta) = 0, \quad (15)$$

where $\Pi^2 = \sum_{i,j} (\partial_{x_i}\beta_j)^2 = \theta^2/\mathcal{N}$ with $\mathcal{N} = 1, 2$ and 3 at the centers of configurations with planar, cylindrical and spherical symmetry, respectively. Therefore, in the spherical top-hat model, the equations (15), (10) together with the equations relating a , τ , Ω and f are sufficient to determine

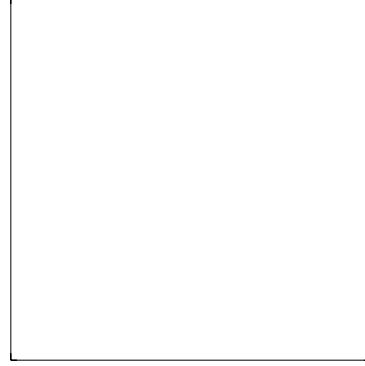


Figure 1. The quantities δ and θ versus the time τ for a positive perturbation for various values of Ω_0 and λ_0 as indicated in the figure. The upper steeply rising and the lower curves, respectively, correspond to bound and unbound perturbations in the $\Omega_0 = 0.2$ cases. The values of δ at the turnaround radii of the bound perturbations are 4.5, 6.7 and 11.5 for $(\Omega_0, \lambda_0) = (1., 0)$, $(0.2, 0.8)$ and $(0.2, 0)$ respectively.

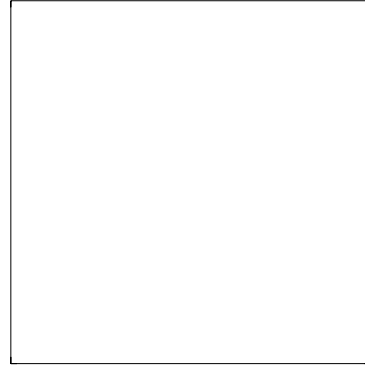


Figure 2. The same as figure 1 but for negative perturbations. The δ curves are almost indistinguishable.

the evolution of the quantities θ and δ . For $\Lambda = 0$, the spherical collapse model can be solved analytically (e.g. Peebles 1980) if the initial peculiar velocity is neglected. Here we numerically integrate the equations (14) and (17) under the initial conditions, $\delta_i = \theta_i$ with $|\delta_i| \ll 1$, where the subscript i refers to quantities at the initial time. These initial conditions are realistic as they arise naturally in linear theory (e.g. Peebles 1980).

In figures 1 and 2 we show the density contrast versus the time τ for positive ($\delta_i > 0$) and negative ($\delta_i < 0$) tophat perturbations for three background cosmologies: $(\Omega_0, \lambda_0) = (1, 0)$, $(0.2, 0.8)$ and $(0.2, 0)$. Figure 1 shows curves for two values of the initial density contrast corresponding to bound and unbound perturbations for the $\Omega_0 = 0.2$ cosmologies. Although the equations were integrated from $\tau = -5.4$ to 0, for the sake of clarity, figure 1 shows results only for $\tau > -1$. For bound perturbations, the growth of δ and θ is

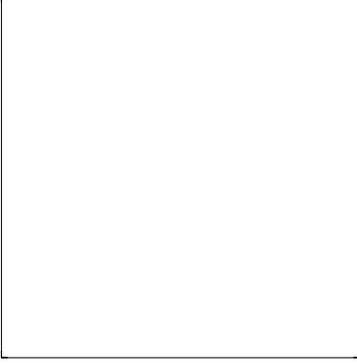


Figure 3. The density parameter versus the time τ for an open universe (dashed line) and a flat universe with a cosmological constant (solid line).

fastest in the open universe case, ($\Omega_0 = 0.2$, $\lambda_0 = 0$). However, significant deviations appear only when δ is larger than 10 or so. This is consistent with the work of Peacock and Dodds (1996) who found that nonlinear effects in the evolution of power spectra in N-body simulations are stronger in an open universe than in a flat $\Omega + \lambda$ universe of the same Ω . Although the $\Omega + \lambda = 1$ case shows more rapid evolution than the $\Omega = 1$ case, the corresponding curves are very similar even when the densities are larger than their values at turnaround. The reason for this is clear from figure 3 which shows Ω versus τ . For $\lambda_0 \neq 0$ we see that Ω is almost unity until relatively late times. Therefore, until late times, the evolution of δ and θ is very similar to the $\Omega_0 = 1$ case. For positive unbound and negative perturbations, the effect of the cosmology on the evolution of δ is almost negligible. The θ curves show some differences. In voids, θ grows more slowly in the low Ω_0 models once the density contrast approaches -1 . Since perturbations in flat universes with a cosmological constant evolve similarly to those with $\lambda = 0$, we do not discuss the case $\Lambda \neq 0$ further.

The top-hat model can be used to evaluate how the variance of an evolved generic density fluctuation field depends on Ω . We require here that the density field is smoothed on large enough scales such that shell-crossing is removed. Curves of $\delta(\Omega < 1)$ versus $\delta_1 \equiv \delta(\Omega = 1)$ satisfy the following (empirical) relation

$$\delta(\Omega) = \delta_1 \exp \left[\frac{\delta_1}{\Delta(\Omega)} \right], \quad (16)$$

where

$$\Delta = \frac{85}{\epsilon(1 + \epsilon)}. \quad (17)$$

This relation works remarkably well for $0.1 < \Omega < 1$ and $\delta_1 < 400$. For generic configurations we assume that the relation (17) is still valid. However we should take into account the fact that the “dimensionality” of the collapse affects the amplitude of the Ω dependence; for example in the one dimensional collapse, before shell crossing, the equations are

free of Ω . Therefore, we replace Δ , in (17), with $4\Delta/(\mathcal{N} - 1)^2$ where \mathcal{N} is the “dimensionality” of the collapse at each point in space. Other than for purely symmetric configurations, the quantity \mathcal{N} is somewhat ambiguous. One possibility is to define it at any point in space in terms of the eigenvalues of the initial velocity deformation tensor, say, as the ratio of the square of the sum of the eigenvalues to the sum of their squares. Nevertheless, for our purposes it is not crucial to specify the form of \mathcal{N} and we simply treat it as a factor which depends on the local topology of the density field. If P is the probability distribution function of the field δ_1 evolved with $\Omega = 1$, then it can be shown that the variance, $\sigma^2(\Omega)$, of the field $\delta(\Omega)$ is given by

$$\sigma^2(\Omega) = \int P(\delta_1) \frac{1 + \delta_1}{1 + \delta(\Omega)} [1 + \delta(\Omega)]^2 d\delta_1 - 1, \quad (18)$$

where we have introduced the ratio $(1 + \delta_1)/(1 + \delta)$ to account for the change in the volume element as a result of the change in density. By expanding (16) to third order in δ_1 and substituting the result in (18) we find

$$\frac{\sigma^2(\Omega)}{\sigma_1^2} = 1 + \frac{1}{a_N \Delta} + S_3 \left(\frac{1}{2} + a_N \Delta \right) \frac{\sigma_1^2}{a_N^2 \Delta^2}, \quad (19)$$

where σ_1^2 is the variance of the field δ_1 and $a_N = 4/(\mathcal{N} - 1)^2$ where $0 < \mathcal{N} < 3$ is some number describing the dimensionality of typical collapse configuration. Note that, in deriving the last relation, we have neglected any local correlation between \mathcal{N} and δ_1 . The factor should depend on the power spectrum of the initial fluctuations and it can be determined empirically from N-body simulations.

Consider now the effect of changing Ω_0 on the dynamics in shell-crossing regions in the case of 1-dimensional collapse. This case is particularly instructive since solutions ($\beta = \mathbf{g}$) to the 1-dimensional equations of motion are fully independent of Ω until the occurrence of shell-crossing. Unfortunately, even in the simple one dimensional collapse, we have no analytic solutions in shell-crossing regions. Therefore we first use the Zel’dovich solution until the formation of the first singularity. Then we switch on to a one-dimensional N-body code to move particles according to (13) in the shell-crossing phase. The initial density field we choose is $\delta_i \propto \cos(x)$. Results of simulations with $\Omega_0 = 1$ and $\Omega_0 = 0.2$ without a cosmological constant are shown in figure 4. The density profile (upper panel) is more concentrated in the open than in the flat case. This is similar to the behavior of density perturbations in the tophat model discussed above. The distribution and velocities of particles in the open model seem to be more evolved in time than in the flat model.

4 Ω DEPENDENCE IN N-BODY SIMULATIONS

We use N-body simulations to study the Ω dependence under general initial conditions. These simulations are especially useful in orbit mixing regions where, according to (13), the effect is most important.

We ran two simulations having $\Omega_0 = 1$ and $\Omega_0 =$

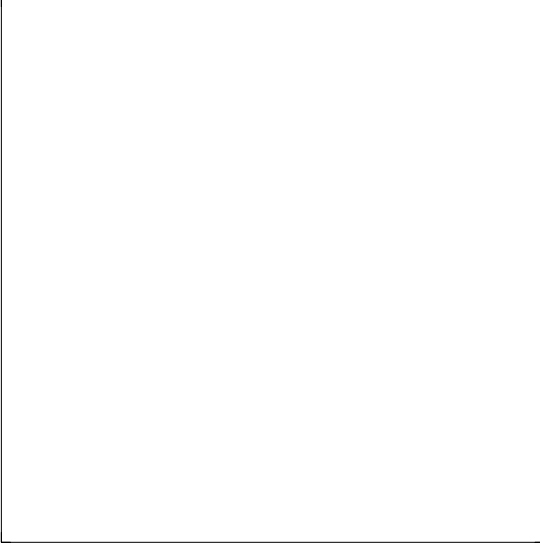


Figure 4. The density profile (upper panel) and the “velocities” (lower panel) in the shell-crossing region in one dimension for $\Omega_0 = 1$ (solid) and $\Omega_0 = 0.2$ (dotted) with no cosmological constant. The initial density perturbation is a cosine wave symmetric about $x = 0$.

0.29 respectively. Both simulations were started from the same initial conditions. The initial conditions were generated from the power spectrum for standard CDM with $H_0 = 50 \text{ km s}^{-1} \text{ Mpc}^{-1}$. Each simulation contained 128^3 particles in a cubic box of length $60 h^{-1} \text{ Mpc}$. The simulations were evolved until the linear *rms* density fluctuations in a sphere of 800 km s^{-1} was 0.5. Both models have roughly the right small scale power as measured by the galaxy pairwise velocity, but produce fewer rich clusters than observed. However, given the scale of our simulations, our choice of the power spectrum and the normalisation is appropriate for our purposes. A model with a higher normalisation would result in too much merging of smaller objects into a few larger objects. Choosing a steeper power spectrum leads to a similar effect.

The simulations were run using a modified parallel version (MacFarland *et al.* 1997) of Couchman’s P³M code (Couchman *et al.* 1995) which uses explicit message passing. The simulations had a softening parameter of 13.2% the mean particle separation and a mesh size of 512 in one dimension. They were run using 64 processors on the CRAY T3E supercomputer at the Computer Center of the Max Planck Society (RZG), Garching.

Figure 5 shows the particle distribution in a slice of thickness $1 h^{-1} \text{ Mpc}$, in the two simulations. The left and right panels correspond to the flat and open model respectively. The lower panels zoom in on the “clusters” seen near the centers of the upper panels. On large scales (upper

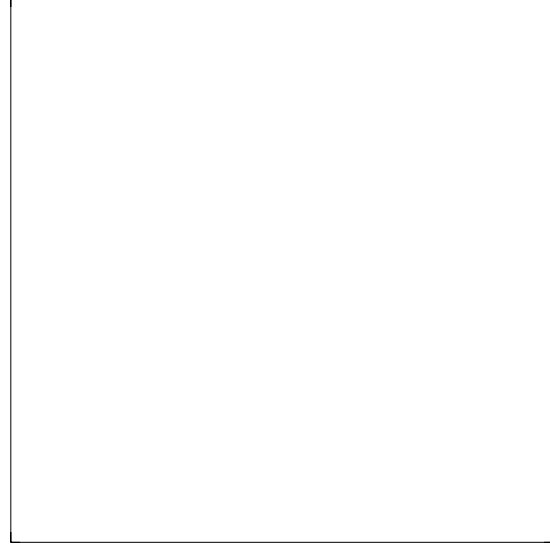


Figure 5. The particle distribution in the low Ω (right) and $\Omega = 1$ (left) simulations. Slice thickness is $1 h^{-1} \text{ Mpc}$. The lower panels focus on the group of “clusters” appearing near the centers of the upper panels.

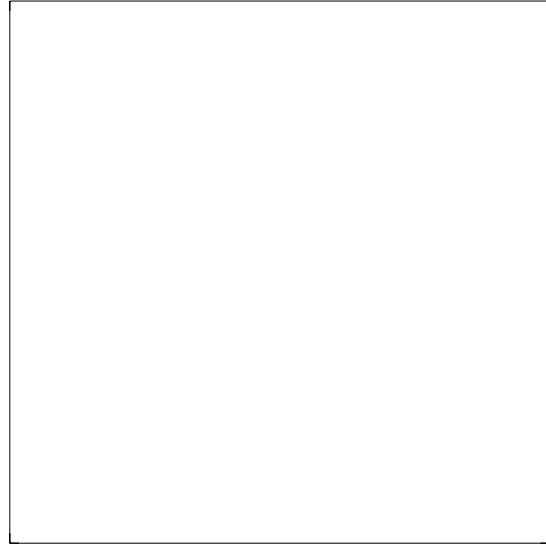


Figure 6. The two point correlation functions for the particle distribution in the two simulations.

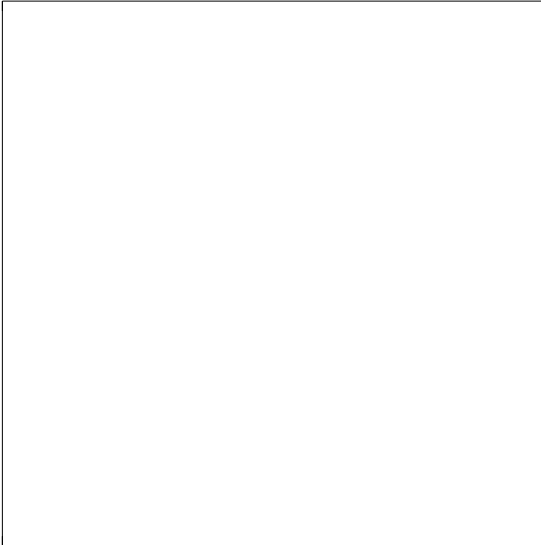


Figure 7. Densities in the open model vs. densities in the flat model. The lower left panel shows densities after the CIC interpolation on a cubic grid of mean particle separation cell size. The other panels show CIC densities smoothed with a top-hat window of width R_s as indicated in the plot.

panels) the two simulations are remarkably similar. Some differences can be spotted in the lower panels. Clusters in the low Ω simulation appear to be more concentrated and evolved. The differences between the two simulations seem to be negligible on scales larger than $1h^{-1}\text{Mpc}$. Indeed the *rms* value of the difference between the positions of the same particles in the two simulations is $0.25h^{-1}\text{Mpc}$ and the largest difference is less than $1.5h^{-1}\text{Mpc}$. The correlation functions for the two simulations, plotted in figure 6, confirm the visual impression from figure 5. The correlation functions differ only on scales smaller than $1.6h^{-1}\text{Mpc}$. On “cluster” scales $\lesssim 0.6h^{-1}\text{Mpc}$ the low Ω correlation function is larger and, on scales $0.6 - 1.6h^{-1}\text{Mpc}$ roughly corresponding to the scale of infall regions around clusters in the simulations, it is smaller than the correlation function in the flat model.

We now quantify the differences between the density and velocity fields. We first use the cloud-in-cell (CIC) interpolation scheme to evaluate the density and velocity fields on a cubic grid of cell length equal to the mean particle separation. This produces a mass weighted average velocity on the grid points. We then further smooth the resultant density and velocity maps with a top-hat filter. In figure 7 we plot the densities in the open vs those in the flat model for 4096 randomly chosen grid points. Even with only CIC smoothing on the grid scale, the correlation between the two density fields is very tight. For densities larger than 10 or so the densities in the open model are larger. The scatter

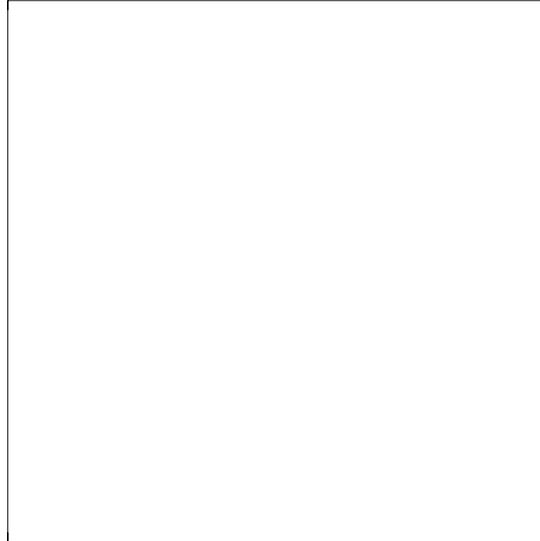


Figure 8. The same as figure 6 but for peculiar velocities. The velocities in the open model were scaled by the factor $f(\Omega_0) = 0.477$.

Table 1. Moments of the density field in the two simulations after CIC and top-hat smoothing of width, R_s , expressed in km/s .

	$\Omega_0 = 1$		$\Omega_0 = 0.29$	
	σ_δ	S	σ_δ	S
CIC	7.331	6.222	8.816	6.374
$R_s = 50$	6.313	5.934	7.397	6.154
$R_s = 100$	3.331	4.855	3.603	5.035
$R_s = 200$	1.693	3.720	1.752	3.833
$R_s = 400$	0.878	3.060	0.891	3.116
$R_s = 800$	0.440	2.549	0.443	2.584

almost vanishes when the density fields are smoothed with a top-hat window of width $> 200\text{km/s}$. Note however that for moderate densities ($0 < \delta < 5$), the densities in the flat model are slightly larger than the open model. This is not surprising since the general tendency is that matter flows out of regions with moderate densities into higher density regions. And since the open model is slightly more evolved, these moderate density regions are somewhat less dense in the open than in the flat model. In table 1 we list the values of the *rms*, σ_δ , and the reduced skewness, $S \equiv \langle \delta^3 \rangle / \sigma_\delta^4$ of the density fields as a function of the smoothing scale. It appears, from the table, that the dependence of S on Ω is stronger than what is predicted from second order perturbation theory (Bouchet *et al.* 1992). That theory is, however,

valid only for $\sigma < 1$. We can use table 1 to determine \mathcal{N}_{eff} in (19) which relates σ_δ in an open universe to that in an $\Omega = 1$ universe. A comparison of (19) with table 1 suggests that $\mathcal{N}_{eff} \approx 2$. This value is reasonable since non-linear collapse configurations are likely to have pancake-like shapes. Recall that the simulations were stopped when the linear value of σ_δ smoothed with a top-hat filter of width $R_s = 800\text{km/s}$ was 0.5. The actual value computed from the simulation is very close to 0.44 in the two simulations. Thus, even though nonlinear effects are clearly important, the difference between the σ_8 in the open and flat simulations is negligible. We now consider the evolved velocity fields. Figure 8 compares one of the components of the velocity fields in the two simulations. The velocity fields in the open model are scaled by the factor $f(\Omega_0)$. Even for large velocities and small smoothing widths, the velocity fields in the two simulations seem to be related by the factor f . A close inspection of the scatter plot for $R_s = 400\text{km/s}$ reveals that the slope of the regression of v/f on v_1 is slightly less than unity. This is because large velocities are generally associated with strong nonlinear effects which tend to spoil the scaling by f .

We mentioned at the end of section 2, that the motion of particles in bound objects is independent of Ω in terms of a time variable which corresponds to a velocity which is the peculiar comoving velocity divided by $\Omega^{0.5}$. Therefore we expect the velocity dispersion (*rms* velocity) in groups of particles identified in the simulation to scale, approximately, like $\Omega^{0.5}$. To test this conjecture, we have used a friends-of-friends (f.o.f) algorithm (kindly supplied by A. Diaferio) to identify groups in the simulations. We then computed the one-dimensional velocity dispersion of particles in each group. Figure 9 (upper panel) shows the mean velocity dispersion in groups as a function of the number of particles they contain. Velocities in the plot are scaled by $\Omega_0^{0.5}$ for the open model. It seems that this scaling works well. Given the uncertainties in identifying group members by the f.o.f algorithm, the deviations from this scaling for large groups are not significant. We conclude that while the (smoothed) average velocity of particles scales like $f(\Omega)$, the *rms* velocity, roughly, scales like $\Omega^{0.5}$. It is interesting to compare the abundance of groups in the two simulations. The lower panel of figure 9 is a plot of the abundance as a function of the number of particles for the two simulations. The abundance of groups is slightly higher in the open model. This is easy to understand, because groups in the open model are tighter than groups in the flat model, the f.o.f algorithm naturally assigns more particles to them. Note that observations naturally provide the abundance of groups as a function of the mass. Since the mass of groups with the same number of particles is proportional to Ω_0 , abundance curves, when plotted versus the mass, look significantly different in the two simulations.

5 SUMMARY

We have shown that gravitational dynamics of a pressureless fluid in an expanding universe is almost independent of the cosmological parameters. According to the equations of motion, expressed in terms of the linear growing mode, the

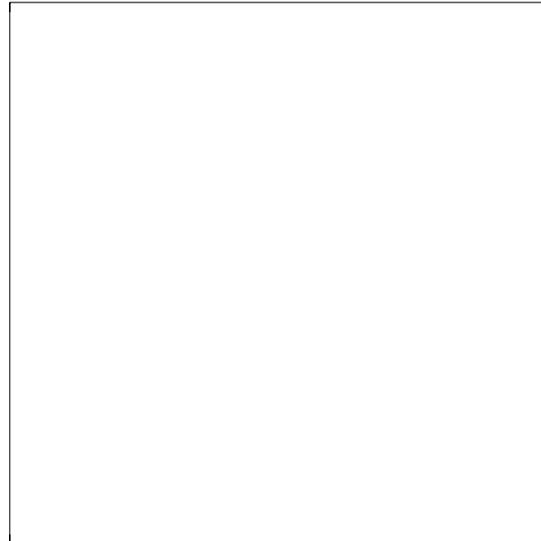


Figure 9. *Top:* The mean 1-D velocity dispersion (*rms* velocity deviations) divided by $\Omega_0^{0.5}$ in groups vs. the number of particles they contain for the two simulations. The lengths of the error-bars give the 1-sigma scatter about the mean for the flat model. The scatter in the open model is similar. *Bottom:* The abundance of groups vs. the number of particles they contain. Groups are identified using a f.o.f algorithm.

final structure in a low Ω model, with or without a cosmological constant, is more evolved than in a flat universe. We used toy-models and N-body simulations to investigate the effect of changing the cosmological background on the evolution of fluctuations and, in particular, on the final velocity and density fields. The present density, when smoothed on scales slightly larger than cluster scale, is almost insensitive to the cosmological background. The background can affect the structure of bound objects (or halos). Halos, characterised by the same ratio of mass to background density, are more centrally concentrated in an open than in a flat universe. However, this effect is weak and is likely to depend on the initial power spectrum. On the other hand, the amplitude of the comoving peculiar velocities of particles strongly depends on Ω . It is remarkable that the smoothed nonlinear velocity field scales with the growth factor, f , just as it does in linear theory.

Since f depends very weakly on the cosmological constant, the final velocity field is mainly sensitive to Ω . Therefore the observed peculiar velocity and density fields in the nearby universe contain information only on Ω (Lahav *et al.* 1991). However, constraints on both Ω and Λ can, in principle, be obtained by measuring the clustering amplitude at different redshifts, for example via the correlation function (Lahav *et al.* 1991). As we have shown, it is rather difficult to detect signatures of the cosmological background in the structure of density fields. Fortunately, observations provide

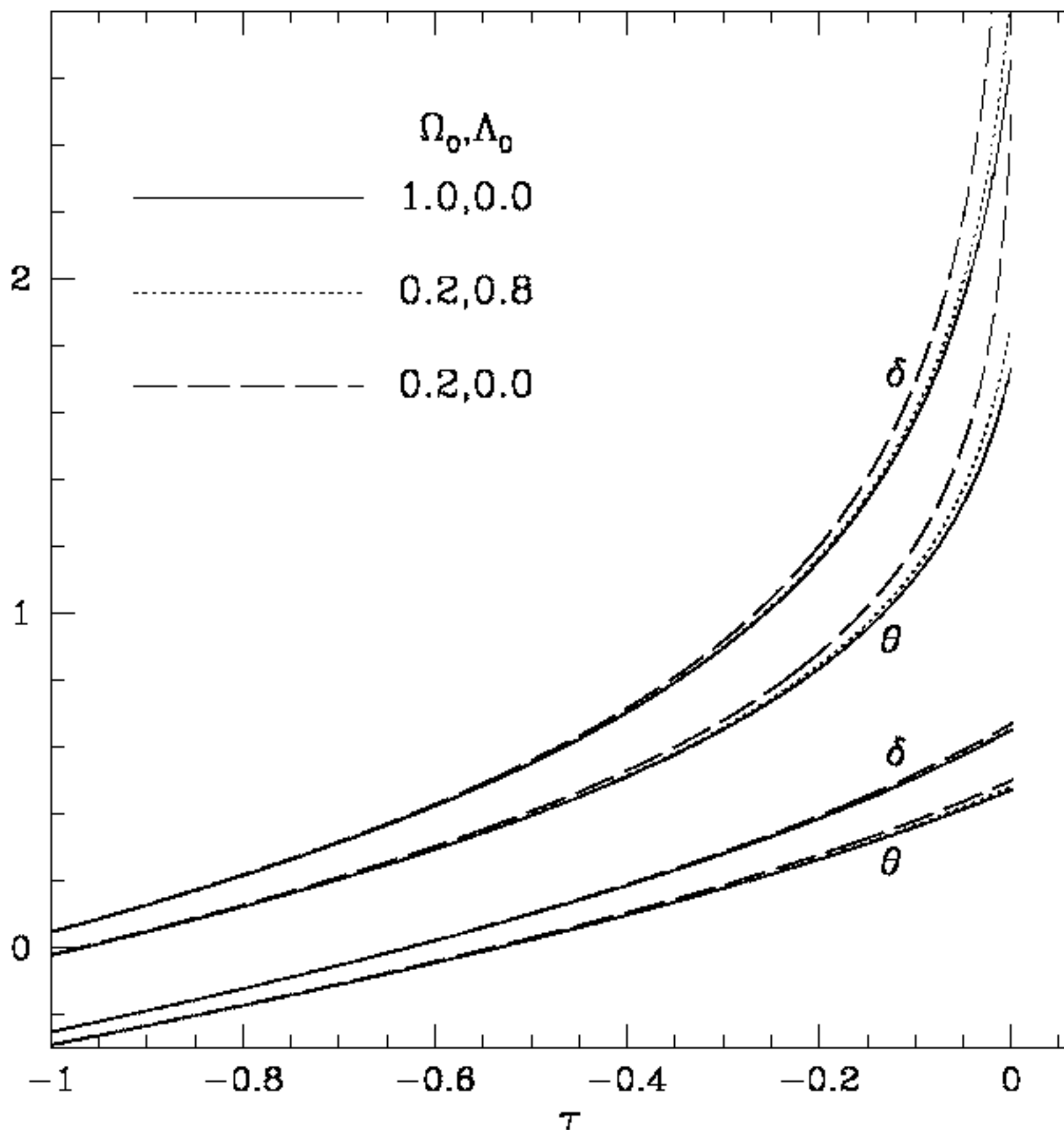
the distribution of galaxies in redshift space. Thanks to the strong dependence of the velocity field on Ω , the anisotropy of clustering in redshift space can provide a measure of Ω . However, such estimates of Ω involve an assumption on the relationship between the distribution of galaxies to that of the dark matter. Estimates of Ω independently of the galaxy distribution can be obtained from the observed peculiar velocity field alone (c.f. Dekel 1994). This makes peculiar velocity catalogs a very powerful tool to constrain the cosmological model. It is especially important for future peculiar velocity measurements to aim at larger sky-coverage and denser sampling rate.

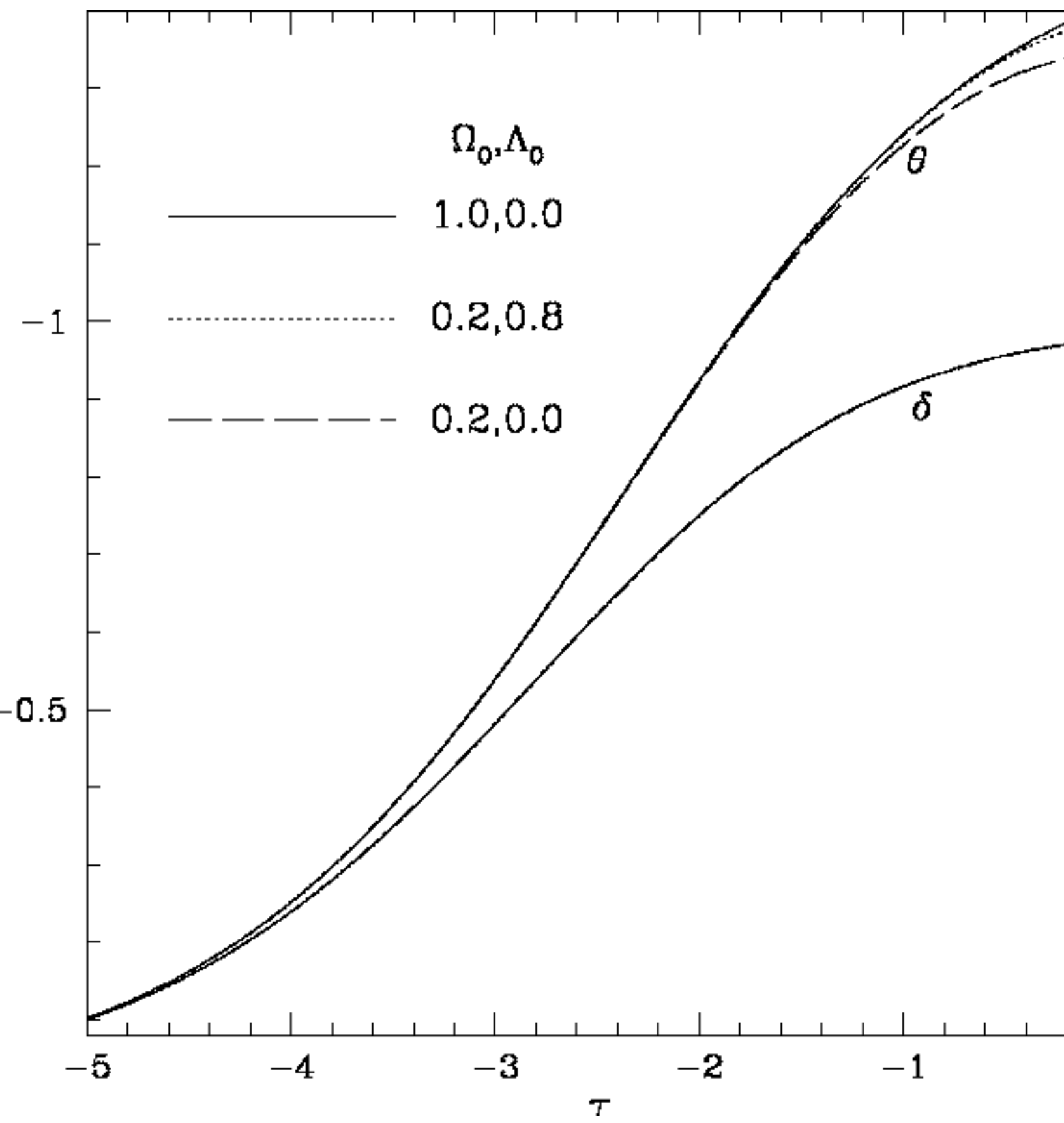
ACKNOWLEDGMENTS

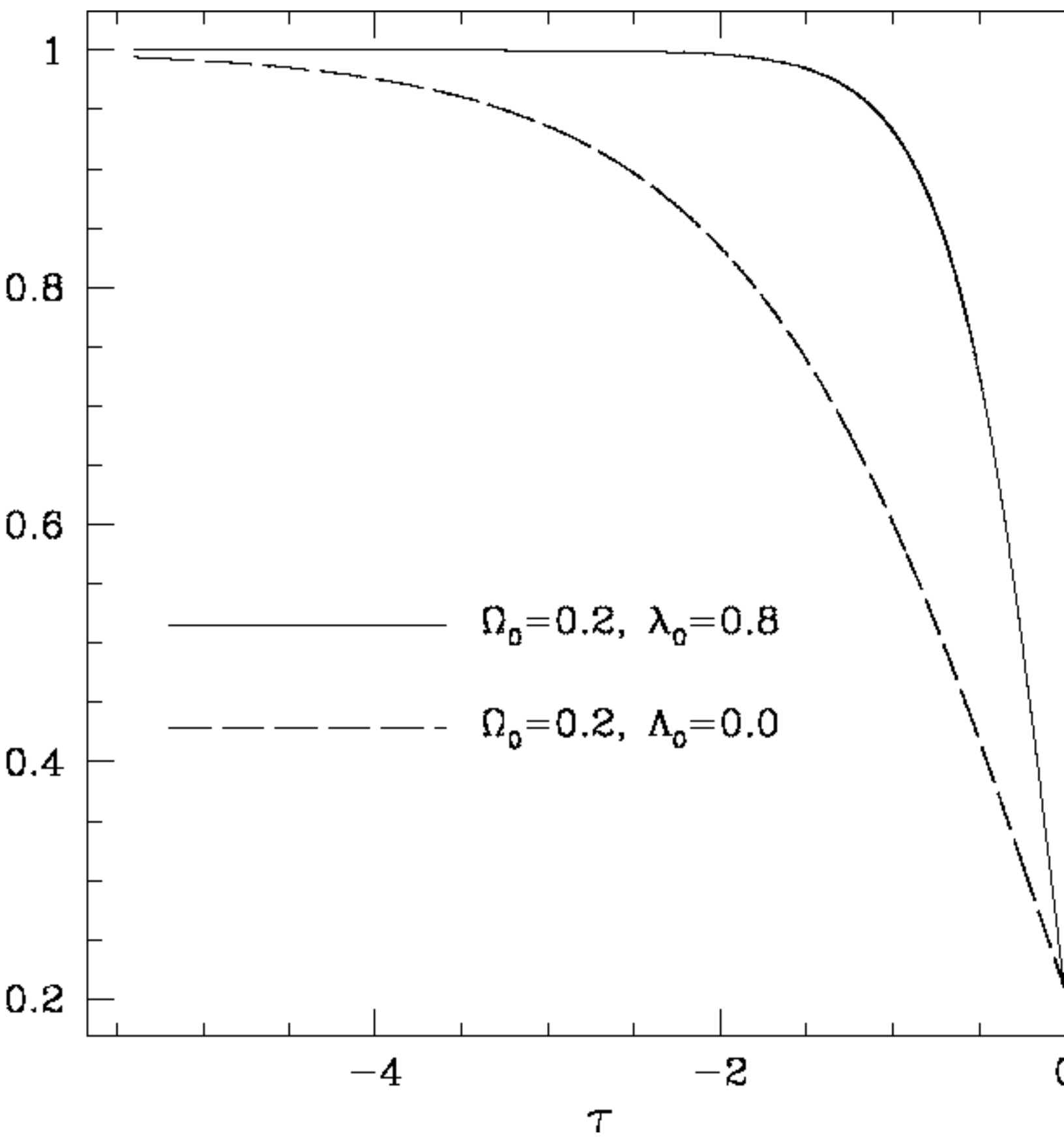
We especially would like to thank Ravi Sheth for many useful comments, and Tom MacFarland for his valuable contributions to running and improving the parallel P3MN-body code. We also thank Simon White for useful discussions, and Antonaldo Diaferio for allowing the use of his group finding code.

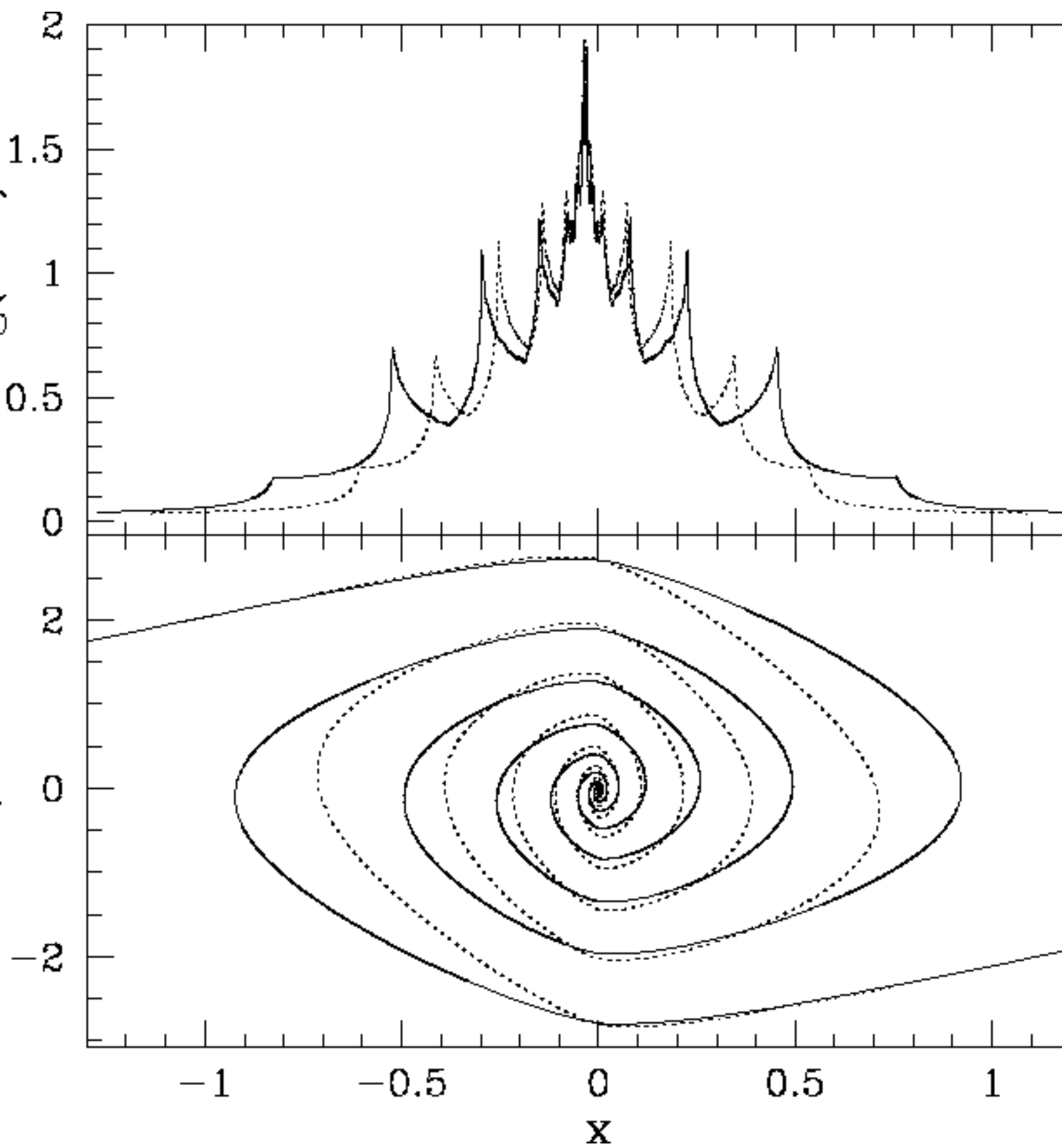
REFERENCES

- Bernardeau, F., Juszkiewicz, R., Dekel, A. and Bouchet, F.R. 1995, MNRAS 274, 20
 Bouchet, F.R., Juszkiewicz, R., Colombi, S. and Pellat, R. 1992, ApJ 394, L5
 Couchman H.M.P., Thomas P.A. and Pearce F.R. 1995, ApJ, 452, 797
 Davis, M., Efstathiou, G., Frenk, C. and White, S.D.M. 1985, ApJ 292, 371
 Heath, D. 1977, MNRAS 179, 351
 Lahav, O., Rees, M.J., Lilje, P.B. and Primack, J.R. 1991, MNRAS 251, 128L
 Lightman, A.P. and Schechter, P.L. 1990, ApJS 74, 831
 MacFarland T.J. *et al.* 1997, in preparation
 Nusser, A. and Dekel, A. 1992, ApJ 391, 443
 Peacock, J.A. and Dodds, S.J. 1996, MNRAS 280L, 19
 Peebles, P.J.E. 1980 *“The Large Scale Structure in The Universe”*, Princeton University Press, Princeton.
 Zel’dovich, Y.B. 1970 A&A 5, 84

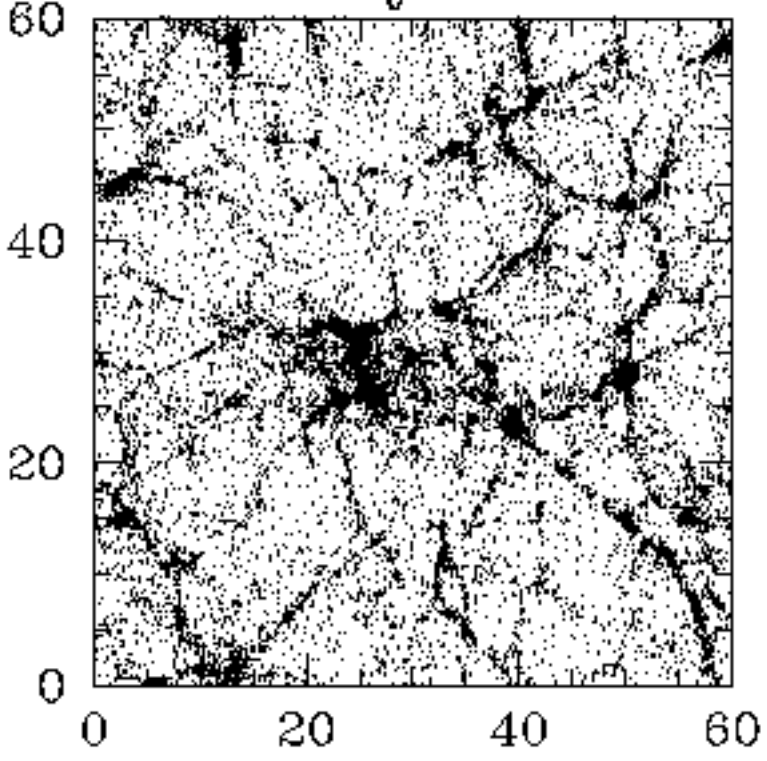








$\Omega_0 = 1$



$\Omega_0 = 0.29$

